metals

MDPI

Article

Analysis of Microstructure and Chip Formation When Machining Ti-6Al-4V

Islam Shyha [1,2,*], Salah Gariani [1], Mahmoud Ahmed El-Sayed [3] and Dehong Huo [4]

1 Department of Mechanical and Construction Engineering, Faculty of Engineering and Environment, Northumbria University at Newcastle, Newcastle upon Tyne NE1 8ST, UK; salah.gariani@northumbria.ac.uk
2 Production Engineering Department, Faculty of Engineering, Alexandria University, 21544 Alexandria, Egypt
3 Department of Industrial and Management Engineering, Arab Academy for Science, Technology and Maritime Transport Abu Qir, 21599 Alexandria, Egypt; m_elsayed@aast.edu
4 Mechanical Engineering, School of Engineering, Newcastle University, Newcastle upon Tyne NE1 7RU, UK; dehong.huo@newcastle.ac.uk
* Correspondence: islam.shyha@northumbria.ac.uk; Tel.: +44-19-1243-7834

Received: 2 February 2018; Accepted: 13 March 2018; Published: 14 March 2018

Abstract: Microstructure and chip formation were evaluated during the step shoulder down-milling of Ti-6Al-4V using a water-miscible vegetable oil-based cutting fluid. Experiments were conducted using the Cut-list fluid supply system previous developed by the authors and a conventional cutting fluid supply system. A thin plastically deformed layer below the machined surface was observed during the metallurgical investigation of the surfaces produced using both systems. Despite noticeable reductions in cutting fluid consumption achieved by Cut-list, no significant disparity was found in microstructural damage. The microstructure of the machined surfaces was strongly affected by cutting speed and fluid flow rate with a discontinuous serrated chip being the principal type. However, increases in cutting fluid flow rate associated with increased cutting speed significantly changed chip morphology where average distance between chip segments increased with cutting speed. Cut-list produced smaller saw-tooth height and larger segmented width, while the transition from aperiodic to periodic serrated chip formation was governed by cutting speed and feed rate. Chip segmentation frequency and shear angle were also sensitive to cutting speed.

Keywords: milling; Ti-6Al-4V; microstructure; chip formation

1. Introduction

The application of cutting fluid plays a vital role in metal cutting processes. Most machining processes cannot be performed effectively without cutting fluids, particularly when cutting refractory materials such as titanium and nickel-based alloys. Cutting fluids also contribute to reducing the contact pressure between the cutting tool and workpiece material and dissipate heat from the machining zone, resulting in extended tool life and reduced power consumption [1]. More details of the benefits, types of cutting fluid, their environmental impacts and supply systems, problems and requirements when machining titanium alloys, as well as the detailed design and fabrication of the new cutting fluid supply system known as Cut-List developed by the authors are available in previous publications [2,3]. This paper presents results related to microstructure and chip formation which have not yet been reported. Therefore, the following discussion considers the relevant literature on these two crucial measures in the machining of titanium alloys.

To establish a high reliability level for critical machined components for aerospace applications, the surface integrity of titanium alloy should be guaranteed, including surface roughness, surface microhardness, microstructure and residual stresses. Thus, the control of surface integrity is of

immense significance in the machining process [4]. For instance, during cutting, the workpiece material is exposed to mechanical, thermal, and chemical energy which can lead to the strain ageing and recrystallisation of the material. Owing to the strain ageing process, the material might become harder and less ductile, while recrystallisation might cause the material to become less hard but more ductile. These mechanical (high stress and strain) and thermal (high temperature and rapid cooling) effects are the chief causes of microstructural alterations, as well as plastic deformation and phase transformation [5]. During the dry turning of Ti-6Al-4V, Che-Haron et al. [6] observed a thin disturbed or plastically deformed layer formed immediately below the machined surface. Prolonged machining using worn tools also produced severe plastic deformation and a thicker disturbed layer on the machined surface. Ginting et al. [4] attributed plastic deformation on the machined surface to the high cutting pressure at elevated temperatures during the dry cutting of titanium alloys. A large plastically affected region below the machined free surface was also observed during the high-speed dry machining of Ti-6Al-4V. The thickness of the deformed layer was found to increase with cutting speed [7]. Severe plastic deformation was also detected on Ti-6Al-4V and Ti-5Al-4V-Mo/Fe alloys after extended drilling. It has been suggested that microstructural alterations are strongly affected by cutting speed and tool wear [8]. Conversely, Armando et al. [9] observed no grain deformation when milling Ti-6Al-4V with a WC/Co. tool under flood cooling conditions. However, when no cutting fluid was supplied, microstructural damage was clear. Ezugwu et al. [10] also reported the absence of any subsurface microstructural alteration during the finish turning of Ti-6Al-4V using polycrystalline diamond (PCD) tools under conventional flood and high pressure cutting (HPC). This was attributed to the small shearing forces due to the sharp cutting edges (new tooling) being insufficient to cause large plastic deformation. In a recent study by Moussaoui et al. [11], noticeable defects and plastic deformation below the machined surface were observed during dry milling. Grain deformation near the machined surface was also apparent when dry turning Ti-6Al-4V. Three deformed regions were identified below the machined surface, as shown in Figure 1. The angle and depth at which the grains were deformed tended to decrease with increasing cutting speed.

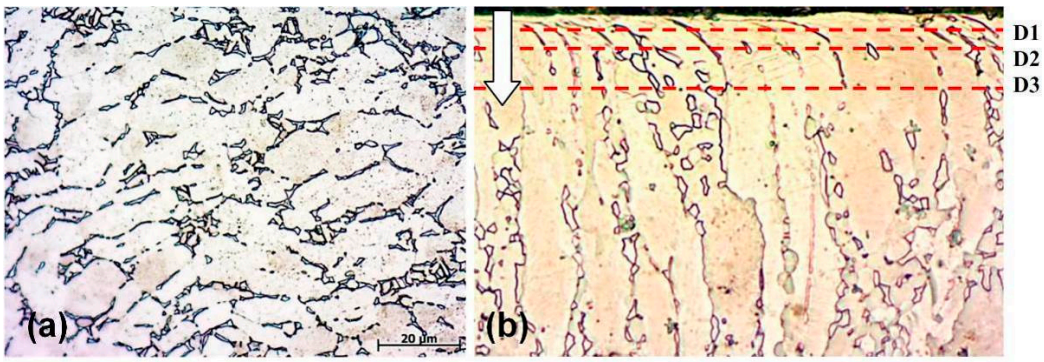

Figure 1. Microstructure of Ti-6Al-4V (**a**) and subsurface deformation regions (**b**) after dry machining of Ti-6Al-4V: D1 (highly deformed region), D2 (moderate deformation) and D3 (unaffected grains), data from [12].

Additionally, residual stresses are considered to be another indicator of surface integrity that can be detrimental to the performance and fatigue life of machined components. Assessment of residual stresses offers a route to design appraisal, failure analysis and quality control. Cutting speed and depth of cut have been found to be the predominant factors affecting induced residual stresses and the flood-cooled turning of Ti-6Al-4V induced compressive residual stresses at low cutting speeds until reaching zero at 145 m/min and subsequently tensile stresses above 145 m/min [12]. It was noted that the tensile transition temperature is strongly affected by cutting conditions (cutting speed, feed rate and depth of cut) as well as the cooling media employed. These findings are in agreement with work by Velásquez et al. [7], who pointed out that the tensile transition occurred at a cutting speed of about

100 m/min when dry turning Ti-6Al-4V, where the drop in cutting speed is believed to be due to the cooling effect. In another study, Mantle et al. [13] highlighted that cutting speed along with tool flank wear have the greatest effects on residual stresses when dry milling gamma titanium aluminide alloy.

Machining processes usually lead to the production of plenty of chips that must be handled efficiently. Chip formation affects cutting temperature and forces, workpiece surface integrity, and tool life. Therefore, it is crucial to determine the preferred cutting conditions that result in chips being easy to handle. This, in turn, could reduce adverse effects on the cutting tool and workpiece surface integrity [14]. Titanium alloys generally produce highly discontinuous segmented or serrated chips owing to their low thermal conductivity [14]. Three theories have been proposed to explain the main reasons for chip segmentation and serration. Firstly, segmented chip formation occurs due to periodic (regular) crack initiation in the free surface of a workpiece due to the high stress and heat generated by friction. The cracks then propagate inside the primary shear zone (possibly at low cutting speed), leading to the separation of the material into two surfaces. Secondly, the formation of segmented chips takes place due to catastrophic or instable thermoplastic shear. This phenomenon occurs due to competition between thermal softening and work hardening in the primary shear zone owing to the high heat generated during machining. This consequently promotes the formation of shear bands [15]. Finally, a combination of the two theories proposes that cracking occurs along adiabatic shear bands at low temperatures <800 °C and strain rates> 1 s^{-1} [16–18]. It has also been reported that cutting speed is the main factor controlling chip segmentation, and the proposed critical cutting speed at which thermoplastic instability occurs is >9 m/min [18]. Theoretically, the degree of segmentation (maximum chip height divided by the continuous partial height of the serrated chip) or serration (G_s) of titanium is also a function of cutting speed (V) according to the equation $G_s = 1.34 \times 10^{-2} \times V^{0.56}$ [19]. On the other hand, Sun et al. [20] underlined that segmented chip formation would cause cyclic cutting forces and tool chatter, which understandably could lead to progressive tool wear. During the dry turning of titanium metal matrix composites (Ti-MMC), Bejjani et al. [21] observed the onset of chip segmentation from a crack on the material's free surface ahead of the tool rather than at the tool tip. Cutting speed was found to significantly affect chip segmentation. Average distances of about 150 µm and 90 µm were recorded between segmented chips at cutting speeds of 50 and 150 m/min respectively. A similar trend was also reported by Sutter et al. [22], who found a decrease in segmentation distance with increasing cutting speed during the dry cutting of Ti-6Al-4V. Yang et al. [19] further confirmed that the degree of segmentation is very sensitive to cutting speed when cutting different metallic materials, including titanium alloys. Additionally, cutting speed and uncut chip thickness had considerable effects on chip segmentation in terms of strain, temperature, and ß volume fraction (the volume per unit volume of the phase or constituent), while other machining parameters such as tool rake angle, tool radius, and friction coefficient were found to have less impact [23,24]. Although chip segmentation frequency and length are commonly used to quantify chip segmentation, Atlati et al. recently introduced a new measure named segmentation intensity ratio (SIR) [25]. SIR is a ratio between two successive adiabatic shear bands where the effect of cutting conditions and tool geometry (rake angle) on the chip segmentation intensity can be quantitively analysed. It was concluded that SIR is very sensitive to cutting conditions (particularly cutting speed and feed rate) when cutting an aeronautical AA2024–T351 alloy. Increasing cutting speed results in higher strain localisation in the adiabatic shear bands. At low feed rates, the chip persists continuous regardless of the used cutting speed and tool geometry. Nevertheless, for high feed rates, tool rake angle strongly influences the chip morphology [25,26]. Harzallah et al. [27] proposed another effective method to quantify the chip segmentation phenomenon called metric segmentation frequency where the metric frequency of segmentation can be measured in segment per millimeter under different machining conditions. It was found that metric frequency of segmentation strongly depends on cutting conditions and tool geometry in particular rake angle.

Additionally, as the intended aim of machining is to separate a certain layer from the rest of the workpiece with minimum possible plastic deformation and thus less energy consumption. Therefore,

the plastic deformation in machining must be reduced in order to increase the process efficiency. Chip morphology can be quantitively analysed using chip compression ratio (CCR). CCR is considered as one of the crucial indicators that can be used to estimate the amount of plastic deformation in the produced chip [28]. In addition to the traditional technique used to determine CCR (i.e., the actual chip thickness, t_2 divided by the uncut chip thickness, t_1), Asthokov et al. [28] suggested another effective method known as weighting method to quantify actual chip thickness (t_2) based on the equation $t_2 = G \times L_c \times b_c \times \rho \times g$ where G is chip weight, L_c and b_c are the measured chip length and width respectively, ρ is the density of the work material and g is the gravity constant.

In previous work by the present authors [2], their new Cut-list system showed superior machining performance compared to conventional systems, particularly in terms of reductions in cutting fluid consumption (42%), cutting force (16%), tool flank wear (46.77%), and burr formation (31.70%).

The novelty of this study is its comparison of performance of the new supply system (Cut-list) and a conventional flood system in terms of surface microstructural damage and chip formation during the shoulder milling of Ti-6Al-4V. Both systems were evaluated at similar operating conditions using water-miscible VO-based cutting fluid.

2. Design of the New Controlled Cutting Fluid Impinging Supply System (Cut-List)

Figure 2 shows the configuration of the Cut list system. A closed loop coolant pump, cutting fluid filters, digital fluid flow meter/regulator, and digital and dual-scale pressures gauges are the main components utilised in developing the new design. Figure 3 shows the system set-up and the main parts employed to supply cutting fluid to the machining zone, including an angled overhead nozzle ring, nozzle mounting wedges, adjustable nozzle holders and round coherent nozzles. Additionally, the Cut-list nozzles were designed and manufactured based on the geometry of the Webster round coherent nozzle [29]. Unlike the traditional sloped nozzle, the internal curving geometry of the coherent nozzle can generate a coherent jet stream to provide low dispersion and minimum entrained air within the jet [30]. These unique features enhance the penetrability of Cut-list during the cutting process. More details of the design procedure of the new supply system can be found elsewhere [2].

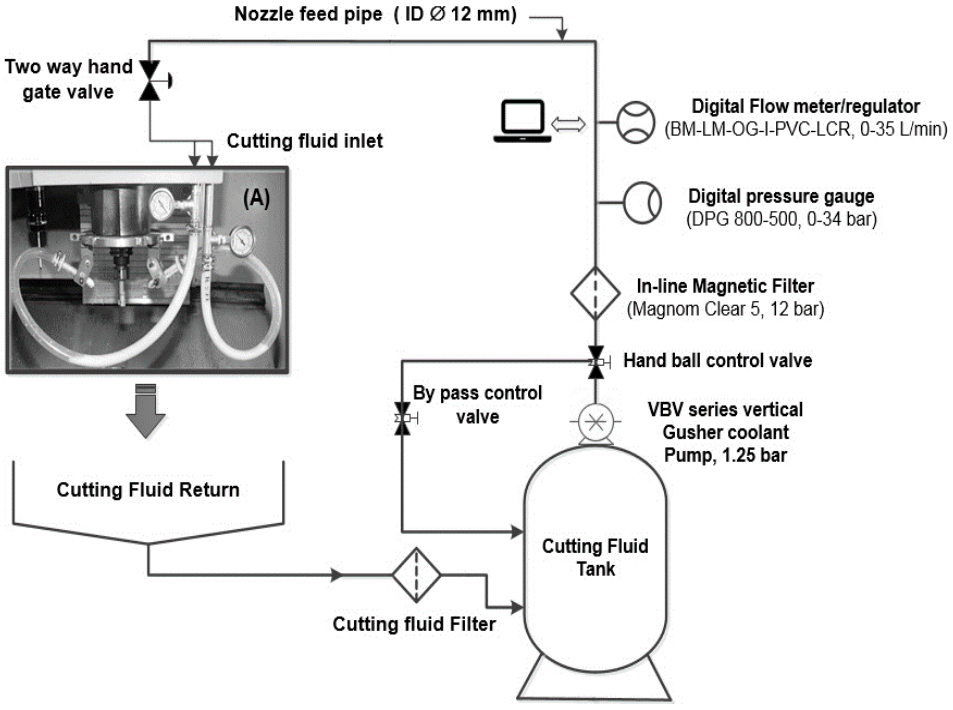

Figure 2. Configuration of the developed Cut-list supply system, data from [2].

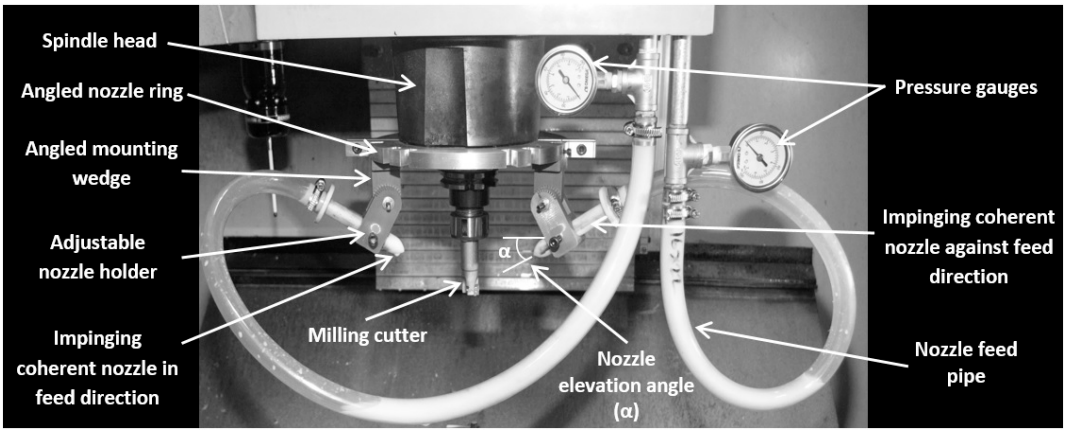

Figure 3. The Cut-list set-up (details of view A).

3. Determination of Parameters of the Fluid Supply System

The shoulder or side-milling process is one of the most common metal removal operations in the machining industry due to its versatility and efficiency. It is widely used in the manufacturing of various general engineering parts as well as when machining critical large titanium components for aerospace and aircraft applications [31]. Thus, the shoulder milling of Ti-6Al-4V alloys was employed in this research, as shown in Figure 4. During metal cutting, a greater proportion of the cutting power consumed (i.e., 90–98%) is converted into heat, whereas the remaining power is retained as elastic energy in the chip [32–35]. In the present work, about 90% of the total cutting power is considered to be converted into the total heat generated in the primary, secondary and tertiary deformation zones. Computations for the new system, including metal removal rate (MRR) and cutting power for determining the accurate flow rate required in each set of cutting conditions, have been detailed in a previous paper [2]. Table 1 shows the cutting conditions used for accurate flow rate calculations.

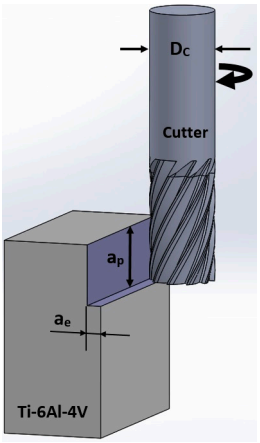

Figure 4. Schematic view of step shoulder milling of Ti-6Al-4V (D_c is the cutter diameter, a_p and a_e is the axial and radial depth of cut respectively).

Table 1. Cutting conditions and levels used for accurate flow rate computation.

Cutting Conditions	Corresponding Levels
Cutting speed (m/min)	95, 200
Feed rate (mm/rev)	0.1, 0.15
Axial depth of cut, a_p (mm)	5
Radial depth of cut, a_e (mm)	1.3

Additionally, conventional flood estimations were based on 13 L/min per kW for cutting titanium as recommended by the Kennametal tools manufacturer [36]. The results show that the fluid can be supplied at a flow rate of 8 L/min per kW using the new Cut-list, with a reduction in cutting fluid consumption by up to 42% compared to the conventional system as shown in Figure 5. These findings, along with calculations of cutting fluid velocity and the minimum aperture diameter of the round coherent nozzle used in this work, have also have been presented earlier [2]. To fulfil the flow coherency criterion, the contraction ratio (D/d) should be at least 2:1 and the actual nozzle aperture diameter (d) must be at least the theoretical minimal coherent nozzle aperture diameter [37]. To obtain the highest jet stream quality, the nozzle dimensions values (d = 1.75 mm, D = 12 mm and D/d = 6.85:1) were kept constant for all trials.

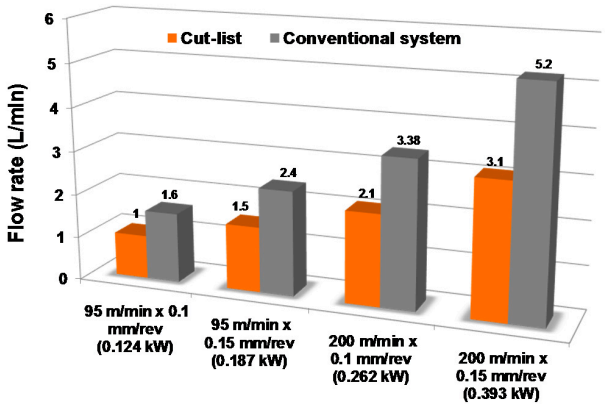

Figure 5. Flow rate versus cutting condition and generated heat for the two supply systems.

4. Experimental Work

The experimental work focused on the analysis of surface microstructure and chip types produced when machining Ti-6Al-4V using two different cutting fluid supply systems (Cut-list and a conventional system) at various machining conditions. Because the new system has the capability for more settings compared to any conventional system, Cut-list was initially evaluated at 3 impinging angles in the feed direction, 3 impinging angles against the feed direction and 3 stand-off/impinging distances, giving 27 tests at four different combinations of machining conditions (2 cutting speeds and 2 feed rates). This gives 108 experiments conducted using the new system and each test was carried out only one time. Out of the 108 experiments, only the trial that gave the best responses in terms of lowest cutting force and workpiece temperature (see the previous report [2] for more detail) were used for comparison with the conventional system relating to microstructural alteration and chip formation. Additionally, the conventional system was tested in four different trials, where cutting speed and feed rate were investigated at two levels each: 95, 200 m/min and 0.1, 0.15 mm/rev respectively. Nozzle elevation angle (α) was set at 40° for all trials. Table 2 shows the factors evaluated with their corresponding levels. All experiments were carried out utilising a 3-axis CNC Cincinnati 750-Sabri vertical machining centre (Cincinnati Machine UK Ltd., Birmingham, UK) with maximum spindle speed and power of 6000 rpm and 11 kW respectively. Workpiece materials used in the machining experiments were titanium α + ß annealed grade 5 rectangular pieces with dimensions of 11 mm × 25 mm × 103 mm. Each trial involved cutting a length of 103 mm with a new sharp tool for each experiment in order to maintain the same cutting conditions. Radial (a_e) and axial (a_p) depths of cut and nozzle elevation angle (α) were kept constant at 1.3 mm, 5 mm and 40° respectively. The cutting tools used were Sandvik H13A coarse grain uncoated carbide inserts. More details of the experimental set-up and process variables used have been presented previously [2]. All trials were performed in wet cutting conditions employing a commercial Vasco1000 (Jemtech (UK) Ltd., East Sussex, UK) water-soluble vegetable oil-based cutting fluid. The cutting fluid concentration was always 10%.

Table 2. Process variables and corresponding levels.

Factor	Leve 1	Level 2	Level 3
Nozzle angle in feed direction	15°	45°	60°
Nozzle angle against feed direction	15°	45°	60°
Nozzle impinging distance (mm)	35	55	75
Cutting speed (m/min)	95	200	-
Feed rate (mm/rev)	0.1	0.15	-

In order to conduct the surface microstructure tests, samples resulting from the optimal cutting conditions in terms of cutting force, *R*a and workpiece temperature were carefully cut-out from the middle of the workpiece with dimensions of 6 mm × 10 mm × 11 mm, (see Figure 6) using a Sodi-Tech EDM wire machine (Sodi-Tech EDM Ltd., Coventry, UK) (<Ø 0.5 mm copper wire). All samples had the same dimensions and were taken from similar locations. The sections were Bakelite-mounted in a Struers LaboPress-3 mounting press. Wet grinding was completed on a SAPHIR350 wet polisher (Aptex Ltd., Solihull, UK) using Ø 300 mm abrasive silicon carbide papers. Fine polishing was accomplished on a Struers LabPress-2 polishing machine (Struers Ltd., Rotherham, UK) using Ø 200 mm 6 µm and 1 µm polishing cloths. A corresponding grit size diamond compound and water-based polycrystalline suspension were used for each stage. The prepared sections were vibratory polished for 6 hours on a Buehler Vibromet-I fine polishing machine (Buehler, Coventry, UK) using a Struers OP-S Non Dry suspension. The sections were consequently swabbed etched on Kroll's reagent for 10 s. The nominal composition of the etchant comprised 6 mL HNO_3 (Nitric acid), 800 mL H_2O (distilled water), and 3 mL HF (Hydrofluoric acid). The sections were then gold-sputtered (as they were not mounted in conducting Bakelite) and examined in a Zeiss Sigma Field Emission scanning electron microscope (SEM) (Carl Zeiss Ltd., Cambridge, UK). The images of microstructure were captured for the undeformed (as received Ti-6Al-4V) and deformed zones (i.e., underneath the machined surfaces) at ×2500 and ×5000 magnifications (Titanium Metals UK Ltd, West Bromwich, UK). Additionally, an optical microscope (Nikon UK Limited, Surrey, UK) (Nikon eclipse LV150 with ×20 magnification) was also employed to capture images of some of the machined surfaces. When necessary, the prepared samples were vibratory cleaned using an ultrasonic cleaner (Kemet Int. Ltd., Kent, UK). Additionally, to collect data of their morphology (i.e., colour, shape, texture and geometry), the chips produced during the machining experiments were collected, cleaned using $(CH_3)_2CO$ solution and examined using TESCAN MIRA 3 type SEM at ×6500 magnification and a Leica S6D optical microscope (Microscope Service Limited, Oxfordshire, UK). Five chips were chosen from each supply system at each cutting condition for the measurement and analysis of saw-tooth height, and width, and crack depth as well as average distance between serrated segments.

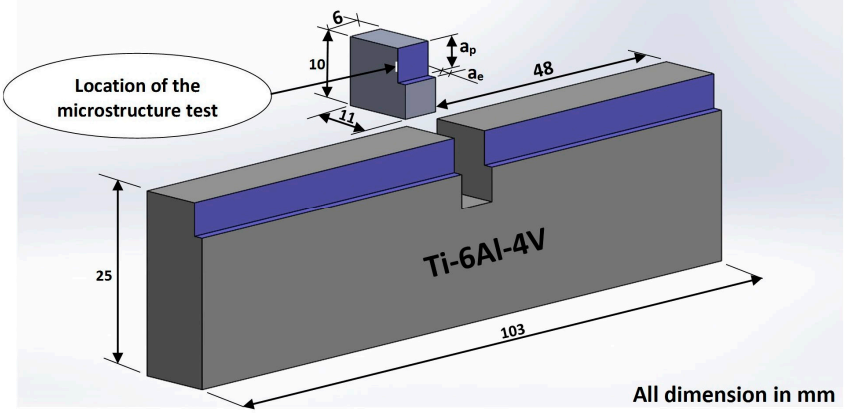

Figure 6. Cut-out of Ti-6Al-4V sample for surface microstructure testing.

5. Results and Discussion

A typical microstructure of an undeformed Ti-6Al-4V alloy, pre-machined, as-received material, is shown in Figure 7, whilst Figure 8 shows the microstructure of post-machining samples. Grains near the undeformed surface, which will be used as the cutting surface, were similar to the rest of grains in the material where typical equiaxed grains were observed, samples of which are shown in red dashed lines. Figure 8 depicts a comparison of the microstructures obtained after using the two different cutting fluid supply systems at different cutting speeds and a feed rate of 0.1 mm/rev. Elongated grains are apparent near the machined surface which is in line with the findings of other studies [12,38]. The boundaries of the deformed layer selected at the end of significant elongation of the grains can be compared with the pre-machined surface equiaxed grain. At 200 m/min cutting speed, the average depths of the deformed layer were 2 µm and 5 µm for Cut-list and the conventional system respectively, as shown in Figure 8b,d. Larger deformed layers 10 µm and 14 µm deep on average depth were obtained at 95 m/min cutting speed as in Figure 8a,c. This is attributed to the highly plastic deformation layer which occurred due to the increased heat generated at low cutting speeds. The deformation was generally deeper at lower cutting speed for the conventional system. The area below the plastically deformed layer (within the dashed line in Figure 8c) represents the grains unaffected by machining. The thinner deformed layer obtained when Cut-list was used is an indication of a reduction in thermal softening owing to better cooling capability, which usually leads to a reduction in compressive stresses and consequently less machined subsurface defects [5]. A thin white (recast) layer of ~1 µm was also observed when the conventional cutting fluid supply system was used at 95 m/min cutting speed, while a thinner recast layer was only seen when the higher cutting speed was used on the new system, see Figure 8b. These results also contradict the findings of earlier studies when dry cutting was employed [4,6,7]. In the same vein, the intense plastic deformation induced by the cutting process, particularly when the conventional system was used, led to a thinning and elongation of the β phase of the Ti-6Al-4V machined surface [7], as seen in Figure 9. This implies that plastic deformation was greater at low cutting speeds, which is in agreement with other studies [4,6–8]. This behaviour is ascribed to the increase in the calculated cutting fluid flow rate associated with the increase in cutting speed, which also improved the fluid's capacity to dissipate heat from the machining zone resulting in less microstructural change and subsurface damage. Edkins et al. [12] reported similar observations where high cutting speeds inevitably led to less grain rotation and smaller regions of influence when cutting titanium. When higher cutting speeds and more flood coolant are used, the strain rate sensitivity dominates the softening effect in the workpiece material, resulting in less subsurface damage. Titanium alloys are considered to be highly strained materials [18,39]. Only for a few micrometres below the machined surface, titanium exhibited a limited thermal softening, which in turn resulted in a reduction in microhardness below the machined surface. The microhardness of machined surfaces is influenced by recrystallisation and changes in grain size and shape. Alterations in microhardness emanates from changes and typically increases in cutting temperature during machining, given the low heat conductivity of titanium alloys and the high cutting pressure at elevated temperature during chip formation. This results in a competitive process between work hardening and thermal softening which affects the fundamental behaviour of the workpiece material. This process is also affected by the dry or wet cooling conditions. Because there was sufficient coolant and enhanced penetration of the cutting fluid using Cut-list, only limited thermal softening occurred below the machined surface. This resulted in a marginal reduction in the microhardness, at 5.5%, compared with 10.5% for the conventional cutting fluid supply system [40].

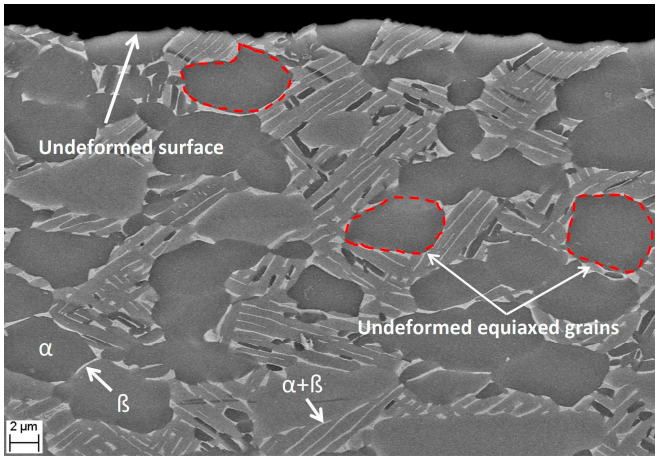

Figure 7. Typical microstructure of undeformed surface of Ti-6Al-4V (as-received material).

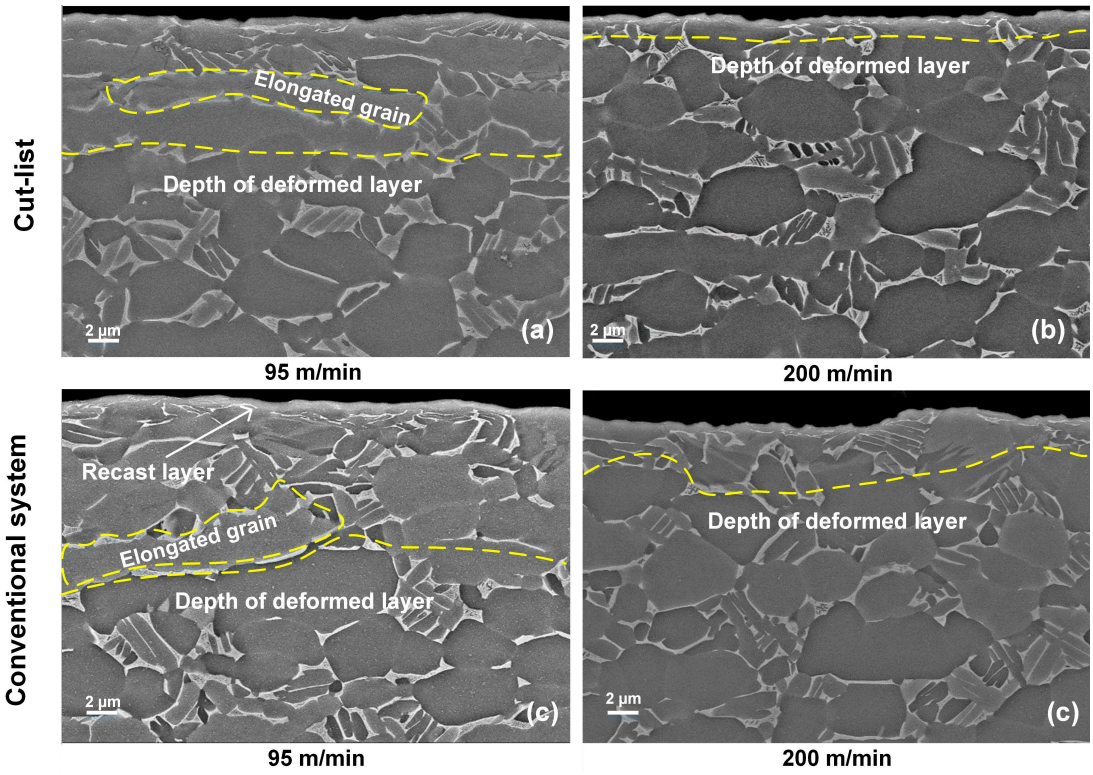

Figure 8. Scanning electron 0microscope (SEM) images of surface microstructure of machined parts at 0.1 mm/rev feed rate using Cut-list at cutting speeds of (**a**,**b**) 95 and 200 m/min respectively and the conventional supply system at cutting speeds of (**c**,**d**) 95 and 200 m/min respectively.

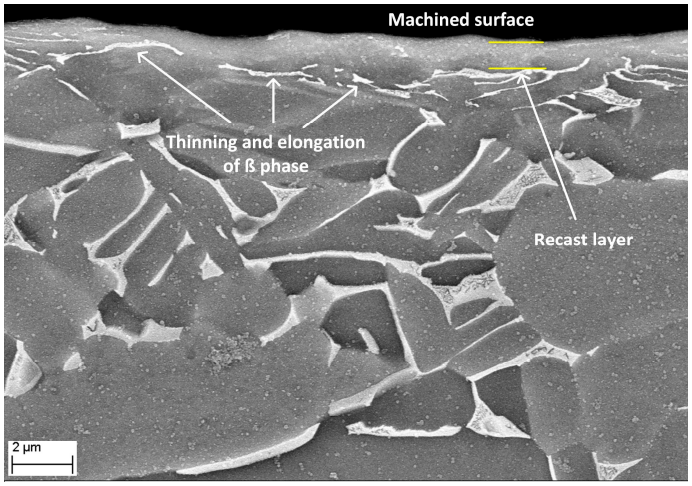

Figure 9. SEM image of thinning and elongation of ß phase (conventional system, 95 m/min cutting speed and 0.1 mm/rev feed rate).

Damage in terms of surface cavities and loss of material was seen only when the conventional flood system was used at higher cutting speeds, as shown in Figure 10. When the carbide cutting insert becomes worn, particles are occasionally separated and adhere to the workpiece surface. This phenomenon is known as carbide cracking, and it promotes a sudden increase in shear stress during machining which leads to surface cavities owing to plucking. This process can generate cavities on the machined surface as well as the erosion of the workpiece material [5,41].

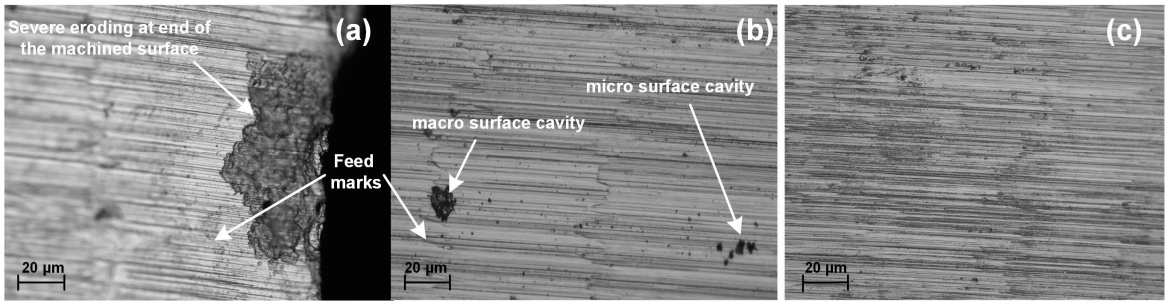

Figure 10. Light microscopic image of the quality of the machined surface: (**a**,**b**) damage when using the conventional supply system; and (**c**) surface produced using Cut-list (all at 200 m/min and 0.15 mm/rev cutting speed and feed rate respectively).

Chips produced throughout the experiments were collected and examined using SEM and a Leica S6D optical microscope to study their morphology (colour, shapes, structures, textures and geometry) and to provide a better understanding of chip formation when Cut-list is employed. Chips produced at the beginning of machining trials were coloured silver-rich. They were thick at the beginning of the cut and became thinner at the end, as shown in Figure 11a. This was due to the use of the climb- or down-milling process, which is more favourable for titanium milling, affording minimum shock load and better tool life compared with the traditional up-milling [15], see Figure 11b.

Figure 12 shows SEM photographs of segmented chips formed by the supply systems. In general, both systems produced similarly desirable nearly curled/C-shape discontinuous segmented chips, particularly at lower cutting speeds, while a nearly flat discontinuous segmented chip shape was generated at higher speeds. In addition, both systems produced chips with different sizes at lower and higher cutting speeds. At lower cutting temperatures, the chips cannot promote the curl due to their increased hardness and lower ductility [42]. This implies that chip morphology is affected by

changes in the volume of cutting fluid delivered into the machining zone as well as changes in cutting speed. Earlier studies also agree [43,44] that chip morphology relies heavily on changes in cutting parameters and the thermal and physical properties of cutting fluids as well as the quantities supplied. In addition, with highly deformed waves on the chips free surface, chip segmentation occurred initially at the lower cutting speed of 95 m/min, which agrees with findings in the literature [45,46]. However, Liu et al. [47] and Daymi et al. [48] reported that chip segmentation was only observed at cutting speeds $\geq$125 m/min during machining Ti-6Al-4V. Relatively irregular (aperiodic) waved-shape segments were seen at 95 m/min whilst partially highly deformed regular (i.e., periodic) waved-shape segments were observed at the higher cutting speed of 200 m/min, see Figure 13. This can be attributed to thermo-plastic instability within the primary shear zone [49].

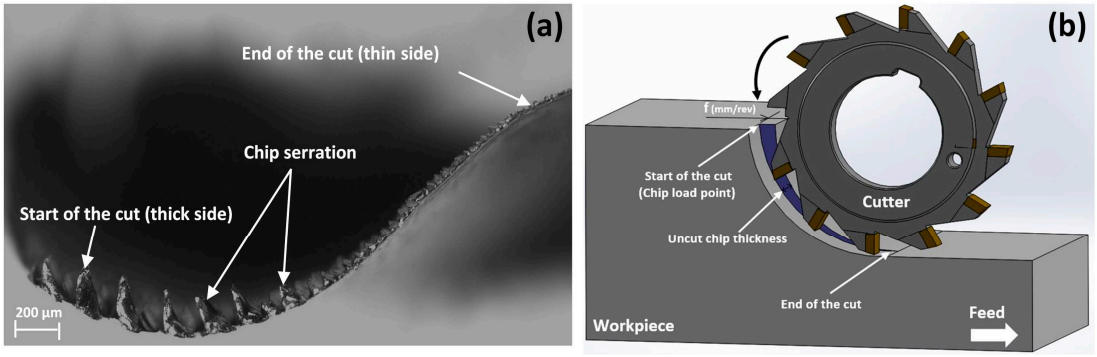

Figure 11. (**a**) Photograph of the produced chip; (**b**) schematic view of down-milling process.

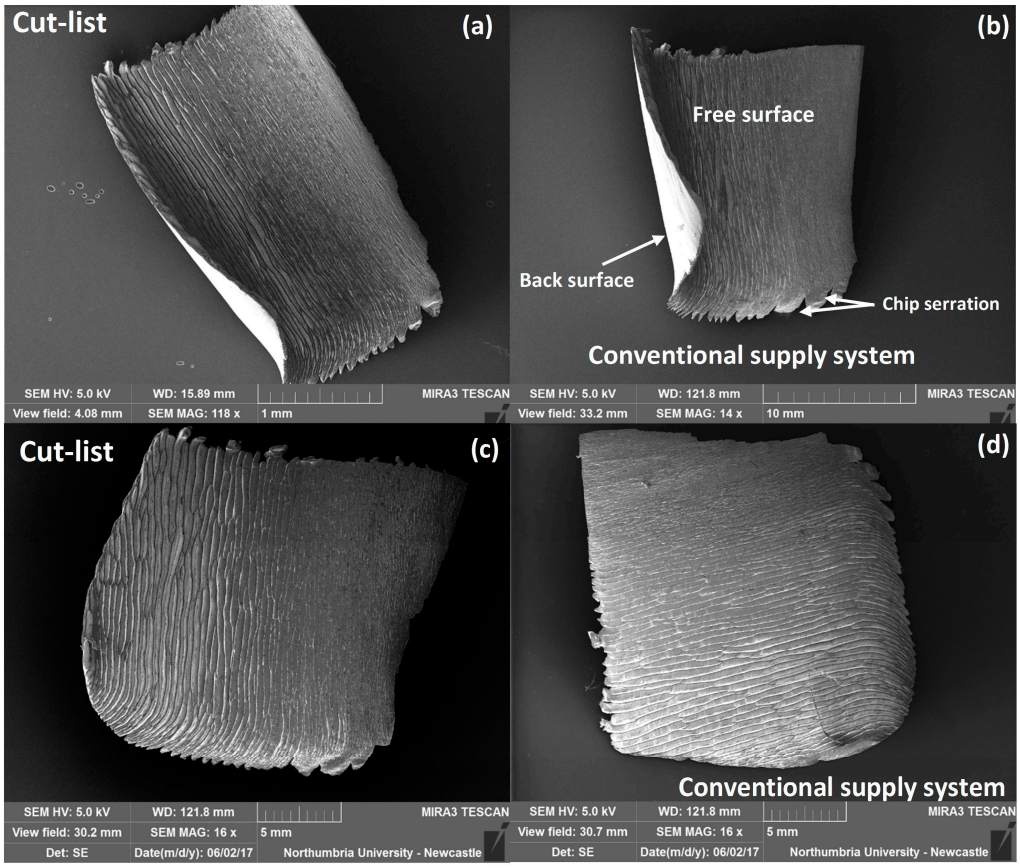

Figure 12. Discontinuous/segmented chips formed at (**a**,**b**) 95 m/min and (**c**,**d**) 200 m/min.

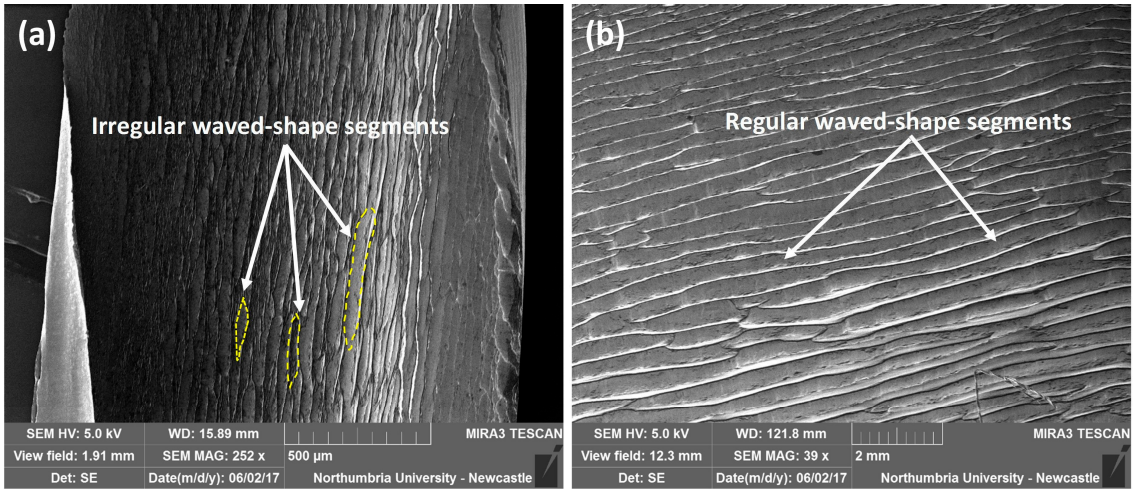

Figure 13. Effect of cutting speed on chip morphology of the free surfaces for Cut-list at: (**a**) 95 m/min; and (**b**) 200 m/min.

The use of the conventional supply system also resulted in larger serration and more crack propagation at the end of the chip-free surface, at lower cutting speed (with a crack depth of up to 200 µm compared with the new system at ~110 µm, as seen in Figure 14). This is due to the large shearing action caused by the inability of the conventional system to effectively deliver a sufficient amount of cutting fluid into the machining zone. Similar trends have been recorded previously [50], where it was concluded that conventional flood cooling induces much serration at the end of the chip-free surface during the milling process owing to its inferior fluid penetrability compared with an MQL supply mode. Furthermore, these results are in agreement with the theory that crack propagation inside the primary shear zone is the main cause of chip serration at low cutting speeds [15]. Figure 15 shows the average crack depth for chips produced by both systems and under various cutting conditions. Five different chips were measured and average values were computed. Error bars are also shown in Figure 15 with a maximum deviation of 2 µm (1%). Additionally, chips generated by both systems have a similarly smooth back surface, which is the surface in contact with the cutting tool rake face. Plastic deformation of the back surface is constrained by the rake face, and consequently it encounters high contact pressure and frictional forces as the chip slides over the cutting tool rake face. The combined effects of frictional forces, high contact pressure and high temperature cause the back surface to be smooth and relatively shiny [51].

Cutting speed has also affected the segmentation characteristics of the chips produced. The average distance between segments is in the range 0.45–0.5 mm and 0.3–0.35 mm for cutting speeds of 95 m/min and 200 m/min respectively, as seen in Figure 16. Similar trends have also been reported during the machining of Ti-6Al-4V, where the segmentation distance decreases with increasing cutting speed [21,46]. This phenomenon can be ascribed to the fact that, as the cutting speed increases, the strain needed to conquer the bonding in materials and to promote a crack decreases. Consequently, smaller segmentation distances are formed [52]. Figure 17 shows the measured average distance between serrated segments for the two systems at various cutting conditions. Larger variation was obtained for the conventional system (0.0156 mm) compared with 0.014 mm for Cut-list as shown in the error bars in Figure 17.

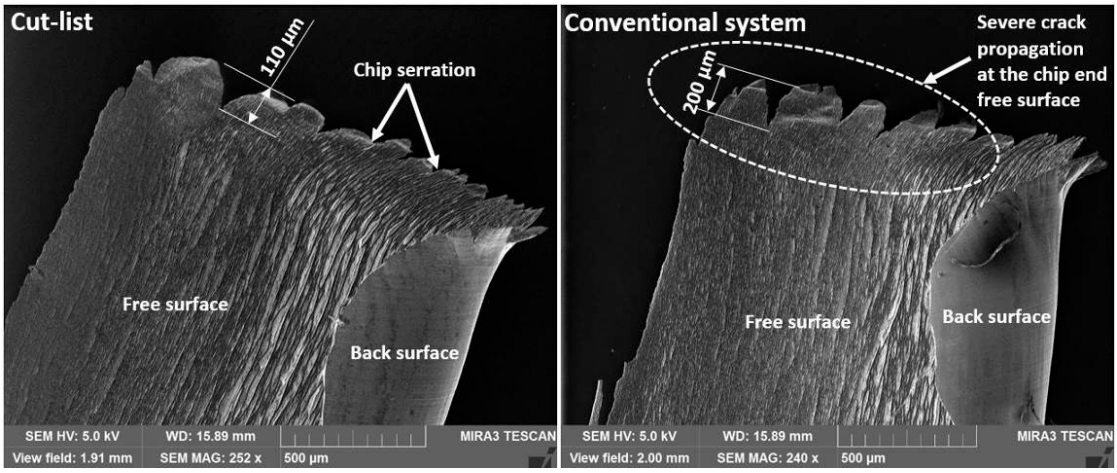

Figure 14. SEM images show serration, back and free surfaces of the chips produced at 95 m/min and 0.1 mm/rev.

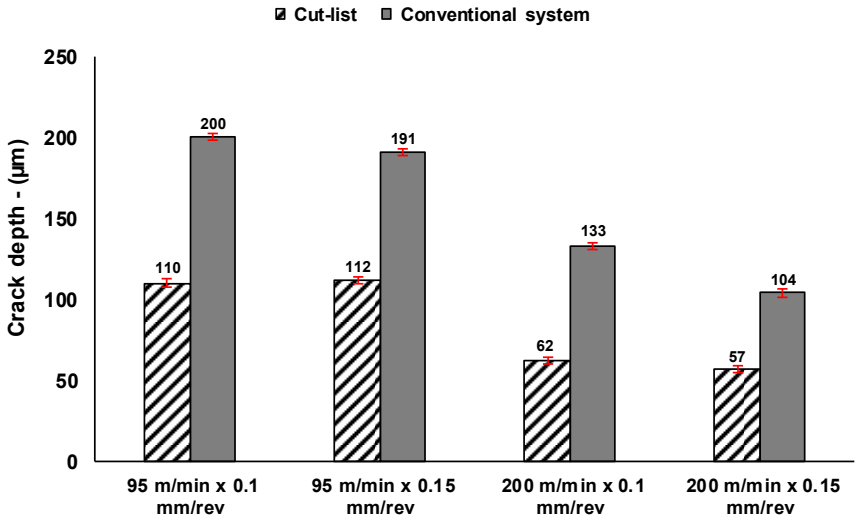

Figure 15. Measured crack depth for different chips under various cutting conditions.

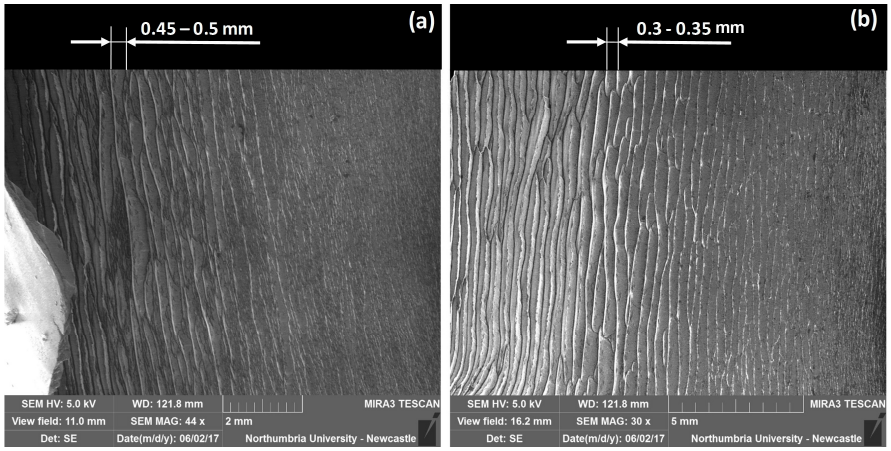

Figure 16. Effect of cutting speed on chip morphology of the free surface: (**a**) 95 m/min; and (**b**) 200 m/min (Cut-list).

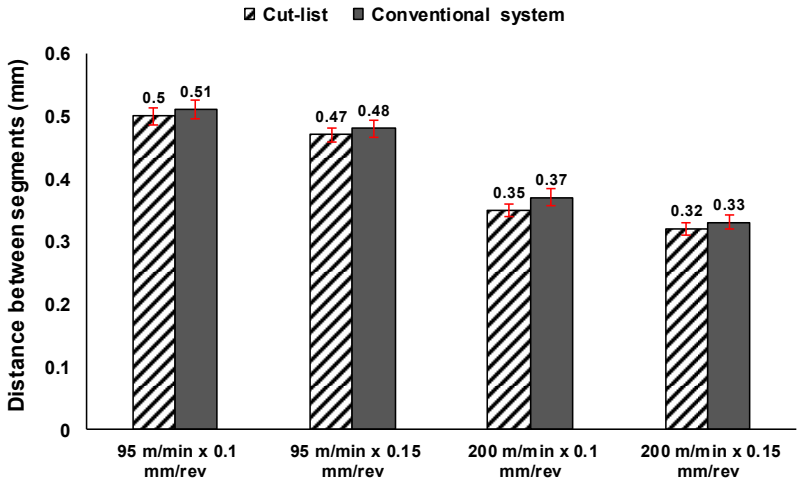

Figure 17. Average distance between serrated segments for the two systems at various cutting conditions.

Figure 18 shows the saw-tooth geometry of the serrated chips generated by the new system at a cutting speed and feed rate of 200 m/min and 0.1 mm/rev respectively. The maximum saw-tooth height (h_{max}) of the serrated chips at various cutting conditions was measured using optical images and the results are presented in Figure 19. Similar variations in h_{max} measurements were seen in Figure 19 (error bars) except at 95 m/min and 0.15 mm/rev when Cut-list values varied with only 0.0017 mm compared with 0.0089 mm for the conventional system. It is observed that h_{max} increases with cutting speed and feed rate for both supply systems with a minimum of 0.117 mm when Cut-list was used. This is also in line with the above conclusion that the use of higher cutting speeds and feed rates can lead to the production of more regular and periodical serration/segmentation profiles in chips. These findings also accord with the conclusion that the transition from aperiodic to periodic saw-tooth chip formation is more affected by increasing cutting speed and feed rate [15,49]. The saw-tooth height (h_{max}) for chips produced using the new system was relatively lower compared with those produced by the conventional supply system. This could be attributed to the better fluid accessibility into the cutting interface provided by the new system owing to a higher fluid velocity up to 10.83 m/s [2], which inevitably leads to the promotion of a short shear area resulting in chips with low saw-tooth height which are also known as thin chips [39,53,54]. Thin chips are more favourable in high quality machining as they can break easily and thus clogging in the tool cutting area is minimised [54].

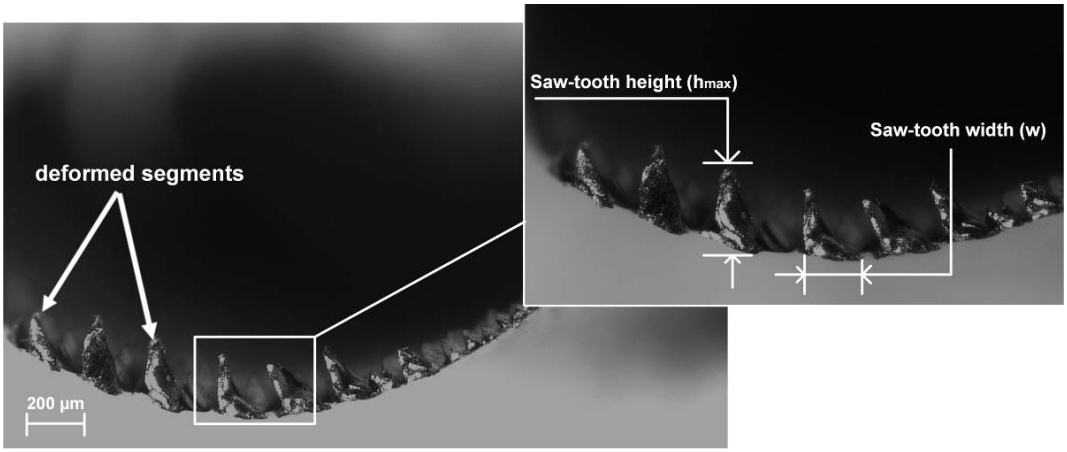

Figure 18. Side view of a deformed chip showing the serration of chips produced using Cut-list at 200 m/min and 0.1 mm/rev.

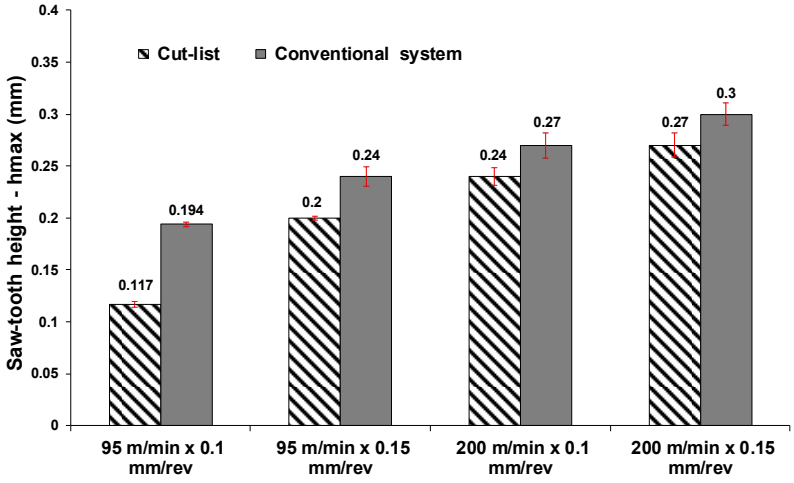

Figure 19. Average saw-tooth height of serrated chips at various cutting conditions.

On the other hand, results for the saw-tooth width (w) of segmented chips are presented in Figure 20. Both systems showed an increase in saw-tooth width with higher cutting speeds and feed rates. This is likely to be due to the competition between thermal softening owing to increased cutting speed and feed rate and the increase in cutting fluid volumes. This helped to reduce shear formation, thus offering larger shear spacing and an increase in segment width. The width of segmented chips was also found to increase, which helped to promote less shear formation during the ultrasonic-assisted turning of Ti-6Al-4V [55]. However, the use of Cut-list resulted in marginally higher segment width owing to its cooling potency. Error bars showed that high measurement variation was observed at 200 m/min and 0.15 mm/rev which were 0.014 and 0.01 for Cut-list and conventional systems, respectively.

Chip segmentation frequency was computed using $f_{\text{chip}} = v/w$ [56], where f_{chip} is the frequency of segmentation in Hz, v is cutting speed in m/s and w is the saw-tooth width of the segment in m. Values for f_{chip} are presented in Figure 21 showing that segmentation frequency clearly increases with cutting speed and decreases with increased feed rate. This tendency is in agreement with findings in the literature [19,56,57]. In addition, all segment frequencies recorded for both supply systems were within the acceptable range of 4–22 kHz for α+ß titanium alloy (Ti-6Al-4V) [56]. The use of Cut-list resulted in reductions in values of f_{chip} at all cutting conditions, with a minimum obtained at 95 m/min and 0.15 mm/rev. Larger variation in the measured data represented in error bars was seen at 200 m/min and 0.15 mm/rev which were 0.842 and 0.721 kHz for Cut-list and conventional system, respectively.

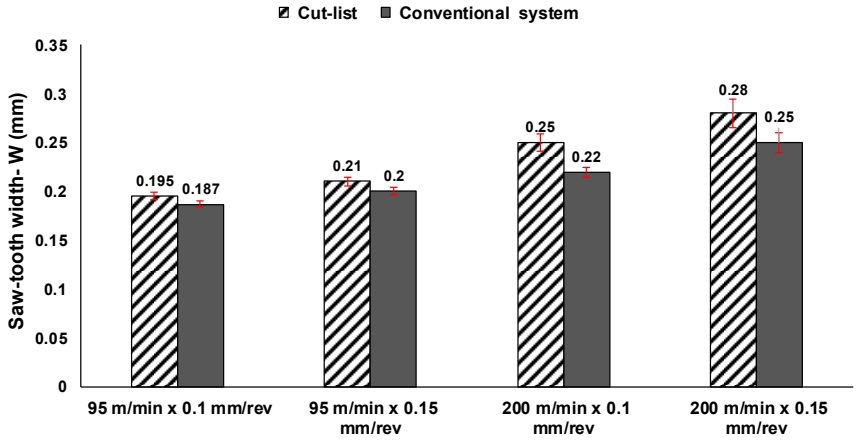

Figure 20. Average saw-tooth width of serrated chips at various cutting conditions.

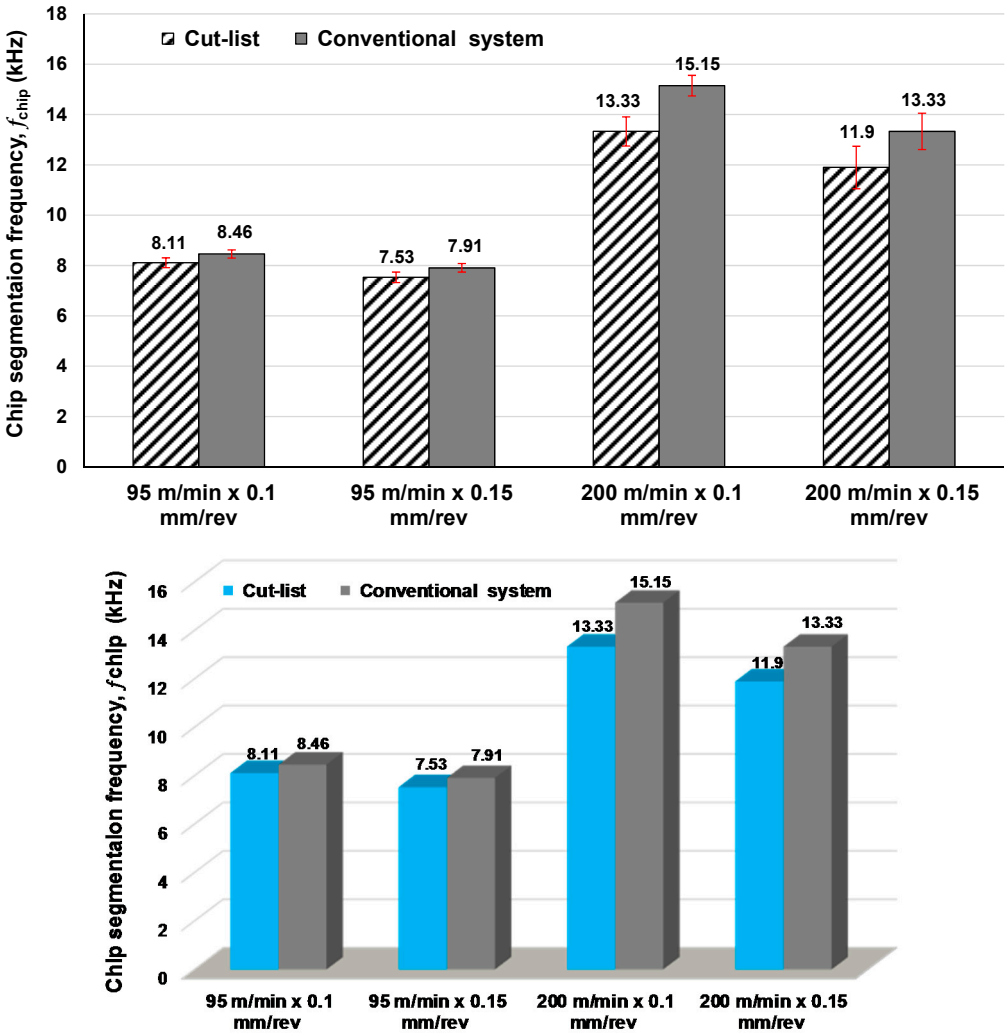

Figure 21. Frequency of segmentation at various cutting conditions for the two supply systems.

Shearing occurs over a very narrow area of the primary shear zone inclined at the so-called shear angle (φ). The shear angle is strongly affected by cutting speed and feed rate [58]. Higher shear angles lead to less deformation along the shear plane, thus resulting in lower cutting forces [54]. The effects of supply system and cutting conditions on shear angle are shown in Figure 22. Both systems showed increases in shear angle with increasing cutting speed. However, limited difference in shear angle between the two systems was observed. This is in agreement with a previous finding [54] that the shear angles caused by high pressure cooling (HPC) were larger than those from dry cutting. Cut-list produced marginally larger shear angles, which can be attributed to the potency of the new supply system where the cutting fluid penetrates effectively into the machining zone and forms a boundary of oil film in the tool-workpiece interface, resulting in lower contact pressure and frictional force. These results can also be explained by the substantial reduction in cutting force (up to 16.41%) when Cut-list was employed compared with the use of conventional systems [2].

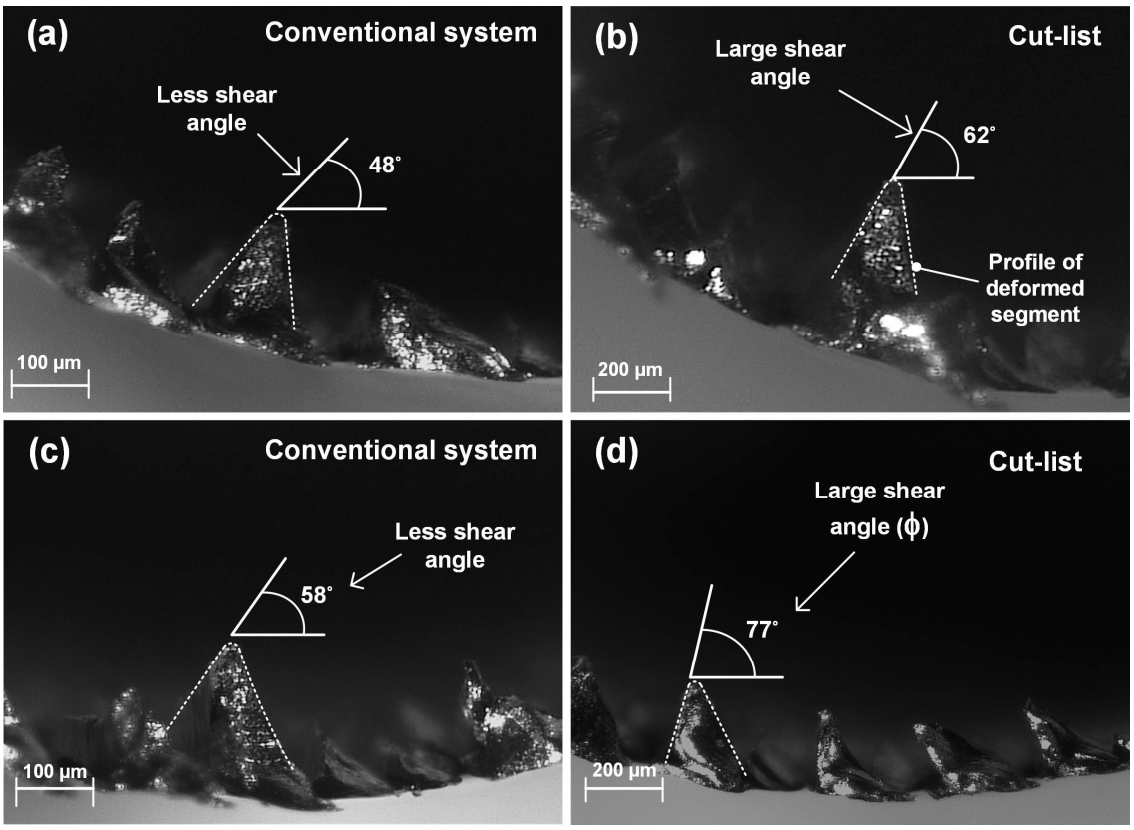

Figure 22. Shear angle (φ) observed at cutting speeds of (**a**,**b**) 95 m/min and (**c**,**d**) 200 m/min.

6. Conclusions

Results related to microstructural alterations and chip formation using two cutting fluid supply systems have been presented, and the main conclusions are as follows:

- Despite the dramatic drop in cutting fluid consumption provided by Cut-list (~42%), less microstructural alteration and a smaller deformed layer below the machined surfaces were observed.
- Cutting speed was a critical factor affecting microstructure, while the increase in cutting fluid flow rate with increasing cutting speeds has helped to mitigate microstructural damage.
- The formation of discontinuous serrated chips is a fundamental characteristic of the down-milling of Ti-6Al-4V with both supply systems under all conditions investigated.
- The free surfaces of all chips generated are characterised by highly deformed wave like-shaped segments, while smooth back surfaces were observed.
- Large crack/serration depths of approximately 200 µm at the end of the chip free surface were observed with the use of the conventional system, compared with only 110 µm for chips produced by Cut-list.
- Cut-list showed decreases of up to 12.5% in chip saw-tooth height (h_{max}) and increases of up to 13.63% in segment width. Segment width was considerably influenced by the volume of fluid supplied to the machining zone, while cutting speed and feed rate played vital roles in the transition from serrated chip formation.
- Increased cutting speed led to increased chip segmentation frequency, while both fluid supply systems presented a typical frequency range of 7.53–15.15 kHz.
- Shear angle (φ) is very sensitive to cutting speed, and larger shear angles were observed when Cut-list was used.

Acknowledgments: The authors would like to thank the Department of Mechanical and Construction Engineering at Northumbria University in Newcastle for the technical support to carry out this research. The authors would also like to thank the Libyan government for financial support.

Author Contributions: Salah Gariani and Islam Shyha conceived and designed the experimental work as well as planned all measurements. Salah Gariani performed the experiments. Measurements and analysis of results were performed by Salah Gariani, Islam Shyha, Dehong Huo and Mahmoud A. El-Sayed. Salah Garaini and Islam Shyha wrote the initial draft of the paper and Mahmoud A. El-Sayed, Dehong Huo participated in writing the results and discussion and revised the whole paper.

Conflicts of Interest: The authors declare no conflict of interest.

References

1. Byers, J.P. *Metalworking Fluids*, 2nd ed.; CRC Press: Hoboken, NJ, USA, 2006; pp. 57–104.
2. Gariani, S.; Shyha, I.; Inam, F.; Huo, D. Evaluation of a novel controlled cutting fluid impinging supply system when machining titanium alloys. *Appl. Sci.* **2017**, *7*, 560. [CrossRef]
3. Gariani, S.; Shyha, I.; Inam, F.; Huo, D. Experimental analysis of system parameters for minimum cutting fluid consumption when machining Ti-6Al-4V using a novel supply system. *Int. J. Adv. Manuf. Technol.* **2018**, *95*, 2795–2809. [CrossRef]
4. Ginting, A.; Nouari, M. Surface integrity of dry machined titanium alloys. *Int. J. Mach. Tools Manuf.* **2009**, *49*, 325–332. [CrossRef]
5. Ulutan, D.; Ozel, T. Machining induced surface integrity in titanium and nickel alloys: A review. *Int. J. Mach. Tools Manuf.* **2011**, *51*, 250–280. [CrossRef]
6. Che-Haron, C.H.; Jawaid, A. The effect of machining on surface integrity of titanium alloy Ti–6% Al–4% V. *J. Mater. Process. Technol.* **2005**, *166*, 188–192. [CrossRef]
7. Velásquez, J.P.; Tidu, A.; Bolle, B.; Chevrier, P.; Fundenberger, J.-J. Sub-surface and surface analysis of high speed machined Ti-6Al-4V alloy. *Mater. Sci. Eng. A* **2010**, *527*, 2572–2578. [CrossRef]
8. Rahim, E.A.; Sharif, S. Investigation on tool life and surface integrity when drilling Ti-6Al-4V And Ti-5Al-4V-Mo/Fe. *JSME Int. J. Ser. C Mech. Syst. Mach. Elements Manuf.* **2006**, *49*, 340–345. [CrossRef]
9. Antonialli, A.Í.S.; Diniz, A.E.; Neto, H.K. Tool life and machined surface damage on titanium alloy milling using different cooling-lubrication conditions. In Proceedings of the 20th International Congress of Mechanical Engineering, Gramado, Brazil, 15–20 November 2009.
10. Ezugwu, E.O.; Bonney, J.; Da Silva, R.B.; Cakir, O. Surface integrity of finished turned Ti-6Al-4V alloy with pcd tools using conventional and high pressure coolant supplies. *Int. J. Mach. Tools Manuf.* **2007**, *47*, 884–891. [CrossRef]
11. Moussaoui, K.; Mousseigne, M.; Senatore, J.; Chieragatti, R.; Monies, F. Influence of milling on surface integrity of Ti6Al4V—Study of the metallurgical characteristics: Microstructure and microhardness. *Int. J. Adv. Manuf. Technol.* **2013**, 1–13. [CrossRef]
12. Edkins, K.D.; Rensburg, N.J.V.; Laubscher, R.F. Evaluating the subsurface microstructure of machined Ti-6Al-4V. *Procedia CIRP* **2014**, *13*, 270–275. [CrossRef]
13. Mantle, A.L.; Aspinwall, D.K. Surface integrity of a high speed milled gamma titanium aluminide. *J. Mater. Process. Technol.* **2001**, *118*, 143–150. [CrossRef]
14. Patil, A.; Sushil, I. Machining challenges in Ti-6Al-4V—A review. *Int. J. Innov. Eng. Technol.* **2015**, *5*, 6–23.
15. Li, A.; Zhao, J.; Zhou, Y.; Chen, X.; Wang, D. Experimental investigation on chip morphologies in high-speed dry milling of titanium alloy Ti-6Al-4V. *Int. J. Adv. Manuf. Technol.* **2012**, *62*, 933–942. [CrossRef]
16. Ducobu, F.; Rivière-Lorphèvre, E.; Filippi, E. Numerical contribution to the comprehension of saw-toothed Ti6Al4V chip formation in orthogonal cutting. *Int. J. Mech. Sci.* **2014**, *81*, 77–87. [CrossRef]
17. Seshacharyulu, T.; Medeiros, S.; Morgan, J.; Malas, J.; Frazier, W.; Prasad, Y. Hot deformation and microstructural damage mechanisms in extra-low interstitial (ELI) grade Ti-6Al-4V. *Mater. Sci. Eng. A* **2000**, *279*, 289–299. [CrossRef]
18. Calamaz, M.; Coupard, D.; Girot, F. A new material model for 2d numerical simulation of serrated chip formation when machining titanium alloy Ti-6Al-4V. *Int. J. Mach. Tools Manuf.* **2008**, *48*, 275–288. [CrossRef]
19. Yang, Q.; Wu, Y.; Liu, D.; Chen, L.; Lou, D.; Zhai, Z.; Liu, Z. Characteristics of serrated chip formation in high-speed machining of metallic materials. *Int. J. Adv. Manuf. Technol.* **2016**, *86*, 1201–1206. [CrossRef]

20. Sun, S.; Brandt, M.; Dargusch, M.S. Characteristics of cutting forces and chip formation in machining of titanium alloys. *Int. J. Mach. Tools Manuf.* **2009**, *49*, 561–568. [CrossRef]
21. Bejjani, R.; Balazinski, M.; Attia, H.; Plamondon, P.; L'Espérance, G. Chip formation and microstructure evolution in the adiabatic shear band when machining titanium metal matrix composites. *Int. J. Mach. Tools Manuf.* **2016**, *109*, 137–146. [CrossRef]
22. Sutter, G.; Faure, L.; Molinari, A.; Ranc, N.; Pina, V. An experimental technique for the measurement of temperature fields for the orthogonal cutting in high speed machining. *Int. J. Mach. Tools Manuf.* **2003**, *43*, 671–678. [CrossRef]
23. Zhang, X.; Shivpuri, R.; Srivastava, A. Role of phase transformation in chip segmentation during high speed machining of dual phase titanium alloys. *J. Mater. Process. Technol.* **2014**, *214*, 3048–3066. [CrossRef]
24. Sutter, G.; List, G. Very high speed cutting of Ti-6Al-4V titanium alloy–change in morphology and mechanism of chip formation. *Int. J. Mach. Tools Manuf.* **2013**, *66*, 37–43. [CrossRef]
25. Atlati, S.; Haddag, B.; Nouari, M.; Zenasni, M. Analysis of a new segmentation intensity ratio "SIR" to characterize the chip segmentation process in machining ductile metals. *Int. J. Mach. Tools Manuf.* **2011**, *51*, 687–700. [CrossRef]
26. Kouadri, S.; Necib, K.; Atlati, S.; Haddag, B.; Nouari, M. Quantification of the chip segmentation in metal machining: Application to machining the aeronautical aluminium alloy AA2024-T351 with cemented carbide tools WC-Co. *Int. J. Mach. Tools Manuf.* **2013**, *64*, 102–113. [CrossRef]
27. Harzallah, M.; Pottier, T.; Senatore, J.; Mousseigne, M.; Germain, G.; Landon, Y. Numerical and experimental investigations of ti-6al-4v chip generation and thermo-mechanical couplings in orthogonal cutting. *Int. J. Mech. Sci.* **2017**, *134*, 189–202. [CrossRef]
28. Astakhov, V.P.; Shvets, S. The assessment of plastic deformation in metal cutting. *J. Mater. Process. Technol.* **2004**, *146*, 193–202. [CrossRef]
29. Webster, J.A. Improving surface integrity and economics of grinding by optimum coolant application, with consideration of abrasive tool and process regime. *J. Eng. Manuf.* **2007**, *221*, 1665–1675. [CrossRef]
30. Rowe, W.B.; Hitchnier, M. *Handbook of Machining with Grinding*, 2nd ed.; CRC Press: Hoboken, NJ, USA, 2007.
31. Wang, F.; Zhao, J.; Li, A.; Zhao, J. Experimental study on cutting forces and surface integrity in high-speed side milling of Ti-6Al-4V titanium alloy. *Mach. Sci. Technol.* **2014**, *18*, 448–463. [CrossRef]
32. Liu, J.; Ren, C.; Qin, X.; Li, H. Prediction of heat transfer process in helical milling. *Int. J. Adv. Manuf. Technol.* **2014**, *72*, 693–705. [CrossRef]
33. Grzesik, W. Chapter nine—Heat in metal cutting. In *Advanced Machining Processes of Metallic Materials*, 2nd ed.; Elsevier: Oxford, UK, 2017; pp. 163–182.
34. Sato, M.; Tamura, N.; Tanaka, H. Temperature variation in the cutting tool in end milling. *J. Manuf. Sci. Eng.* **2011**, *133*, 021005. [CrossRef]
35. Cui, X.; Guo, J. Effects of cutting parameters on tool temperatures in intermittent turning with the formation of serrated chip considered. *Appl. Thermal Eng.* **2017**, *110*, 1220–1229. [CrossRef]
36. Aerospace-Kennametal. Titanium Machining Guide. Available online: https://www.kennametal.com/content/dam/kennametal/kennametal/common/Resources/Catalogs-Literature/Metalworking/Titanium_material_machining_guide_Aerospace.pdf (accessed on 15 April 2016).
37. Morgan, M.; Baines-Jones, V. On the coherent length of fluid nozzles in grinding. *Key Eng. Mater.* **2009**, *404*, 61–67. [CrossRef]
38. Patil, S.; Jadhav, S.; Kekade, S.; Supare, A.; Powar, A.; Singh, R.K.P. The influence of cutting heat on the surface integrity during machining of titanium alloy Ti6Al4V. *Procedia Manuf.* **2016**, *5*, 857–869. [CrossRef]
39. da Silva, R.B.; Machado, Á.R.; Ezugwu, E.O.; Bonney, J.; Sales, W.F. Tool life and wear mechanisms in high speed machining of Ti-6Al-4V alloy with pcd tools under various coolant pressures. *J. Mater. Process. Technol.* **2013**, *213*, 1459–1464. [CrossRef]
40. Gariani, S.; Shyha, I.; Inam, F.; Huo, D. Influence of vegetable oil-based controlled cutting fluid impinging supply system on micro hardness in machining of Ti-6Al-4V. *Int. J. Chem. Mol. Nuclear Mater. Metall. Eng.* **2017**, *11*, 316–321.
41. Zou, B.; Chen, M.; Li, S. Study on finish-turning of $NiCr_{20}TiAl$ nickel-based alloy using Al_2O_3/TiN-coated carbide tools. *Int. J. Adv. Manuf. Technol.* **2011**, *53*, 81–92. [CrossRef]
42. Ravi, S.; Pradeep Kumar, M. Experimental investigations on cryogenic cooling by liquid nitrogen in the end milling of hardened steel. *Cryogenics* **2011**, *51*, 509–515. [CrossRef]

43. Pramanik, A. Problems and solutions in machining of titanium alloys. *Int. J. Adv. Manuf. Technol.* **2014**, *70*, 919–928. [CrossRef]
44. Veiga, C.; Davim, J.; Loureiro, A. Review on machinability of titanium alloys: The process perspective. *Rev. Adv. Mater. Sci.* **2013**, *34*, 148–164.
45. Amin, A.K.M.N.; Ismail, A.F.; Nor Khairusshima, M.K. Effectiveness of uncoated WC–Co and PCD inserts in end milling of titanium alloy—Ti-6Al-4V. *J. Mater. Process. Technol.* **2007**, *192*, 147–158. [CrossRef]
46. Molinari, A.; Musquar, C.; Sutter, G. Adiabatic shear banding in high speed machining of Ti-6Al-4V: Experiments and modeling. *Int. J. Plast.* **2002**, *18*, 443–459. [CrossRef]
47. Liu, H.; Zhang, J.; Jiang, Y.; He, Y.; Xu, X.; Zhao, W. Investigation on morphological evolution of chips for Ti6Al4V alloys with the increasing milling speed. *Procedia CIRP* **2016**, *46*, 408–411. [CrossRef]
48. Daymi, A.; Boujelbene, M.; Salem, S.B.; Sassi, B.H.; Torbaty, S. Effect of the cutting speed on the chip morphology and the cutting forces. *Arch. Comput. Mater. Sci. Surf. Eng.* **2009**, *1*, 77–83.
49. Barry, J.; Byrne, G.; Lennon, D. Observations on chip formation and acoustic emission in machining Ti-6Al-4V alloy. *Int. J. Mach. Tools Manuf.* **2001**, *41*, 1055–1070. [CrossRef]
50. Rahman, M.; Senthil Kumar, A.; Salam, M.U. Experimental evaluation on the effect of minimal quantities of lubricant in milling. *Int. J. Mach. Tools Manuf.* **2002**, *42*, 539–547. [CrossRef]
51. Zhao, Y.; Sun, J.; Li, J. Study on chip morphology and milling characteristics of laser cladding layer. *Int. J. Adv. Manuf. Technol.* **2015**, *77*, 783–796. [CrossRef]
52. Mabrouki, T.; Belhadi, S.; Rigal, J.-F. Fundamental understanding of the segmented chip genesis for smart machining. A contribution in hard material turning. In *Advances in Integrated Design and Manufacturing in Mechanical Engineering II*; Springer: New York, NY, USA, 2007; pp. 443–459.
53. Ezugwu, E.; Bonney, J.; Da Silva, R.; Machado, A.; Ugwoha, E. High productivity rough turning of Ti-6Al-4V alloy, with flood and high-pressure cooling. *Tribol. Trans.* **2009**, *52*, 395–400. [CrossRef]
54. Patil, S.; Kekade, S.; Phapale, K.; Jadhav, S.; Powar, A.; Supare, A.; Singh, R. Effect of α and β phase volume fraction on machining characteristics of titanium alloy Ti6Al4V. *Procedia Manuf.* **2016**, *6*, 63–70. [CrossRef]
55. Patil, S.; Joshi, S.; Tewari, A.; Joshi, S.S. Modelling and simulation of effect of ultrasonic vibrations on machining of Ti6Al4V. *Ultrasonics* **2014**, *54*, 694–705. [CrossRef] [PubMed]
56. Joshi, S.; Pawar, P.; Tewari, A.; Joshi, S.S. Effect of β phase fraction in titanium alloys on chip segmentation in their orthogonal machining. *CIRP J. Manuf. Sci. Technol.* **2014**, *7*, 191–201. [CrossRef]
57. Cotterell, M.; Byrne, G. Dynamics of chip formation during orthogonal cutting of titanium alloy Ti-6Al-4V. *CIRP Ann.* **2008**, *57*, 93–96. [CrossRef]
58. Thamizhmanii, S.; Sulaiman, H. *Machinability Study Using Chip Thickness Ratio on Difficult to Cut Metals by CBN Cutting Tool*; Key Engineering Materials; Trans Tech Publ.: Zürich, Switzerland, 2012; pp. 1317–1322.